Revisiting the ϕ^6 theory in three dimensions at large N

Sandra Kvedaraitė,[1,*] Tom Steudtner,[2,†] and Max Uetrecht[2,‡]
[1]*Departamento de Física Teórica y del Cosmos, Universidad de Granada, Campus de Fuentenueva, E–18071 Granada, Spain*
[2]*Fakultät Physik, Technische Universität Dortmund, D-44221 Dortmund, Germany*

(Received 21 February 2025; accepted 21 August 2025; published 3 September 2025)

We investigate the $O(N)$-symmetric ϕ^6 theory in three spacetime dimensions using dimensional regularization and minimal subtraction. The predictions of other methods are scrutinized in a large-N expansion. We show how the tricritical line of fixed point emerges in a strict $N \to \infty$ limit but argue that it is not a physical manifestation. For the first time in this explicit manner, we compute the effective potential at next-to-leading order in the $1/N$-expansion and discuss its stability. The Bardeen-Moshe-Bander phenomenon is also analysed at next-to-leading order, and we demonstrate that it disappears without breaking the scale invariance spontaneously. Our findings indicate that the UV fixed point found by Pisarski persists at large N.

DOI: 10.1103/tnh4-7lnv

I. INTRODUCTION

In this work, we reinvestigate a theory of N real scalar fields exhibiting an $O(N)$ symmetry in $d = 3$ spacetime dimensions. The most general renormalizable action is given by the Lagrangian

$$\mathcal{L} = \frac{1}{2}\partial_\mu \phi_k \partial^\mu \phi_k - \frac{m^2}{2}\phi^2 - \frac{\lambda}{4!}\phi^4 - \frac{\eta}{6!}\phi^6, \qquad (1)$$

where $\phi^2 \equiv \phi_k \phi_k$ with $k = 1, \ldots, N$. In three dimensions, the coupling η is classically marginal, while both m^2 and λ have positive mass dimension. The model (1) plays a key role in understanding tricritical phenomena, such as those occurring in ^{3}He-^{4}He mixtures [1,2] or the nematic to smectic-A transition in binary liquid crystal mixtures [3,4]. Moreover, (1) is a rare example of quantum field theories (QFTs) in which a nontrivial UV fixed point can be reliably identified using perturbative methods [5–7]. Other such instances include purely fermionic models in three [8–10], and certain gauge-Yukawa theories in four spacetime dimensions [11–15].

In the following, we are interested in the limit where N is very large, allowing for the extraction of nonperturbative results through a $1/N$-expansion. An analysis of the phase structure has been conducted long ago, see, e.g., [5,6,16–18], and is displayed in Fig. 1 in the tree-level approximation. The interaction potential is bounded from below at large field values if $\eta > 0$. Its $O(N)$ symmetry (light gray surface for fixed η) may spontaneously break down to $O(N-1)$ (light blue surface) via a second-order phase transition at $m^2 < 0$ (solid blue line) or a first-order one for $m^2 > 0$ and $\lambda < -\sqrt{8\eta/5}|m| < 0$ (dashed blue line).[1] Along the line of the first-order phase transition, the $O(N)$- and $O(N-1)$-symmetric phases coexist, culminating in a tricritical phase boundary at the intersection with the line of second-order transitions (η axis of Fig. 1).

In this work, we are mostly interested in this phase boundary at $m^2 = \lambda = 0$ for positive values of $\eta > 0$. There are two accounts of the large-N UV behavior of this theory that appear contradictory at a first glance. On the one hand, Ref. [5–7] identified a single UV fixed point using perturbation theory. In particular, Pisarski [7] demonstrated that this fixed point is guaranteed to exist in a systematic $1/N$-expansion (see also [23,24]). On the other hand, it has been argued that in a strict $N \to \infty$ limit, all points $m^2 = \lambda = 0$ exhibit scale invariance [19–21]. This suggests a tricritical line of UV fixed points for all values $\eta \geq 0$ (red line in Fig. 1). Reference [22] showed that this line terminates due to the Bardeen-Moshe-Bander (BMB) phenomenon, which generates a mass scale through nonperturbative effects. This picture is corroborated using saddle point techniques and auxiliary fields in cutoff

*Contact author: skvedaraite@ugr.es
†Contact author: tom2.steudtner@tu-dortmund.de
‡Contact author: max.uetrecht@tu-dortmund.de

[1]Note that transition orders are exchanged in the convention of [16].

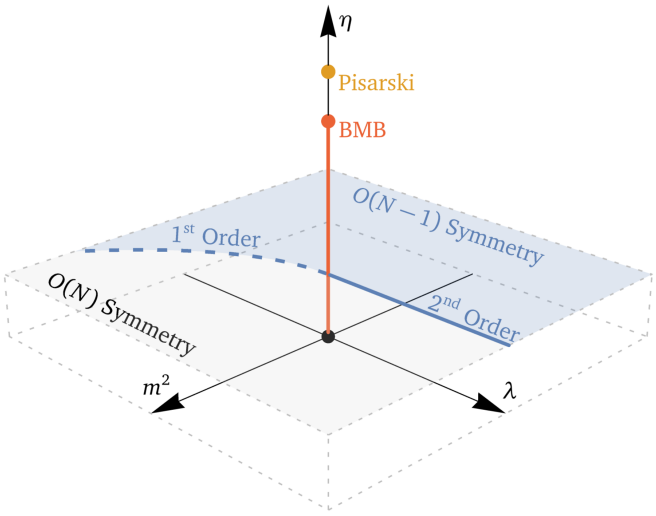

FIG. 1. Schematic overview of the phase diagram for the theory (1). On a slice of a fixed value of η, the unbroken $O(N)$-symmetric phase (light gray surface) and broken $O(N-1)$ symmetry phase (light blue) are shown at tree level. A second-order phase transitions occurs at $\lambda > 0$, $m^2 = 0$ (solid blue line) and a first-order one at $\lambda < 0$, $m^2 = \frac{5}{8}\lambda^2/\eta$ (dashed blue line). Taking quantum corrections into account, a tricritical line of fixed points for $m^2 = \lambda = 0$ and $\eta > 0$ is reported [19–21] in a strict $N \to \infty$ limit (red line). However, the line terminates at the BMB end point (red) [22]. Beyond that line, there is a potential UV fixed point (yellow) found in a $1/N$ expansion [5–7,23].

schemes; see, e.g., [19,20,22,25–28] as well as the functional renormalization group (FRG), see, e.g., [21,29–32]. Pisarski's fixed point (yellow in Fig. 1) lies beyond the BMB end point where scale invariance is broken. Therefore, these nonperturbative arguments appear to suggest that the fixed point does not exist. However, the line of fixed points along with the BMB end point disappears as $1/N$ corrections to the strict $N \to \infty$ limit are considered [19,20,25,30,32]. Pisarski's solution on the other hand survives $1/N$ corrections, but it is unclear if nonperturbative effects still eliminate the fixed point as they do in the $N \to \infty$ limit. In addition, the methods and schemes used to access the tricritical line, BMB phenomenon, and Pisarski's fixed point are quite different and often opaque on a technical level. This makes it difficult to draw a consistent picture about the large-N limit.

In this work, we approach the problem from an accessible, purely diagrammatic angle. Contrary to most previous works, we employ dimensional regularization and the modified minimal subtraction scheme [33–36]. This allows us to make better contact with the high-loop corrections of the renormalization group equations [7,23]. We evaluate the β function and effective potential in a consistent $1/N$ expansion, which involves resumming large families of diagrams in perturbation theory.

With these tools at hand, we investigate the disappearance of the tricritical line, push the expansion of the effective potential to next-to-leading order, and study the implications of the BMB phenomenon.

The remainder of this work is structured as follows: Sec. II reviews Pisarski's fixed point and establishes a controlled large-N expansion. In Sec. III, we argue that the tricritical line is spurious and only exists as an artifact of the $N \to \infty$ limit. We also compute the effective potential at next-to-leading order. To the best of our knowledge, this is the first complete result of its kind in the literature. The BMB phenomenon is scrutinized in Sec. IV, and we demonstrate how it is replaced by stability as $1/N$ corrections are considered. Finally, we collect some concluding remarks in Sec. V.

II. RENORMALIZATION GROUP EQUATIONS

We first consider the renormalization group (RG) evolution in the large-N limit. Note that for dimensional regularization in $d = 3 - 2\varepsilon$, odd loop orders do not exhibit UV divergencies [37]. Thus, β and γ functions in (modified) minimal subtraction schemes only receive contribution at even orders, starting at two-loop. The $\overline{\text{MS}}$ β function of the marginal scalar sextic coupling η has been computed by Pisarski at two and four loops [7] and later extended to six loops in [23]. Retaining only the leading-N terms at each loop order, it reads

$$\beta_\eta = \frac{N\eta^2}{5(4\pi)^2} - \frac{\pi^2 N^3 \eta^3}{7200(4\pi)^4} + c_6 \frac{N^4\eta^4}{(4\pi)^6} + \mathcal{O}(\eta^5), \quad (2)$$

where c_6 is a six-loop constant independent of N; see [23]. We have verified (2) explicitly up to four-loop order. Analyzing the coefficients in (2), we find that in order to absorb the leading powers of N into the coupling η and obtain a finite β function, the sextic coupling should be rescaled [6] as

$$\hat{\eta} \equiv \frac{N^{3/2}\eta}{(4\pi)^2}, \qquad \text{while} \qquad \epsilon \equiv \frac{1}{\sqrt{N}} \quad (3)$$

can be treated as a small expansion parameter. This means that only the four-loop term is leading, while both two- and six-loop contributions are suppressed by a factor of ϵ. In fact, the only diagrams capable of generating the leading-N contributions are[2]

$\beta_\eta =$ 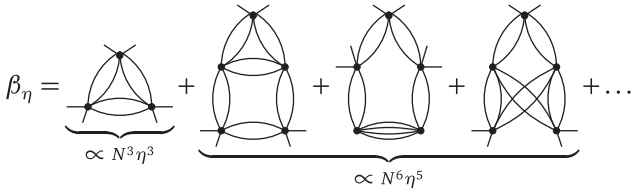 $+ \ldots$

(4)

[2]We are indebted to Ian Jack and Hugh Osborn for pointing out missing eight-loop diagrams.

and appear every four loop orders, while all other orders are suppressed. Keeping only leading-N terms at each loop order, the rescaled β function reads

$$\beta_{\hat{\eta}} = \frac{\epsilon}{5}\hat{\eta}^2 - \frac{\pi^2}{7200}\hat{\eta}^3 + \epsilon c_6 \hat{\eta}^4 + c_8 \hat{\eta}^5 + \ldots. \tag{5}$$

Due to the signs of two- and four-loop terms in (5), a nontrivial UV fixed point emerges [7]

$$\hat{\eta}^* = \frac{1440}{\pi^2}\epsilon + \mathcal{O}(\epsilon^3). \tag{6}$$

In the limit $N \to \infty$ ($\epsilon \to 0$), the fixed point becomes increasingly small and asymptotically free. The coupling $\hat{\eta}(\epsilon)$ can be systematically expanded as a power series in ϵ, where each coefficient is completely determined by $\beta_{\hat{\eta}}$ up to a certain loop order. Thus, higher loops are increasingly suppressed and do not spoil the existence of the fixed point. The coefficient $\propto \epsilon^2$ in (6) vanishes, while next coefficient $\propto \epsilon^3$ requires both the six- and eight-loop parts of the β function, the latter being currently unavailable. This is because the corresponding terms in (5) both give contributions $\mathcal{O}(\epsilon^5)$ at the fixed point.

Furthermore, we provide the eigenvalues of the stability matrix $\vartheta_{1,2,3}$ and field anomalous dimension[3] γ_ϕ^* at the UV fixed point

$$\begin{aligned}
\vartheta_1 &= -\frac{288}{\pi^2}\epsilon^2 + \mathcal{O}(\epsilon^4), \\
\vartheta_{2,3} &= \mp\frac{8\sqrt{3}}{\pi}\epsilon + \mathcal{O}(\epsilon^3), \\
\gamma_\phi^* &= -\frac{96}{\pi^4}\epsilon^4 + \mathcal{O}(\epsilon^5),
\end{aligned} \tag{7}$$

where ϑ_1 corresponds to the $\hat{\eta}$ direction and is UV attractive, while $\vartheta_{2,3}$ are a mixture of the super-renormalizable couplings m^2 as well as $\hat{\lambda} \propto N\lambda$ revealing one attractive and one repulsive direction.

Since the coefficient $\propto \epsilon$ in (6) is positive, we have $\hat{\eta}^* > 0$, which implies that the classical potential is bounded from below. In order to check if this stability persists at the quantum level, we calculate the effective potential next.

III. EFFECTIVE POTENTIAL

In the following section, we compute the effective potential, which incorporates quantum corrections to the classical potential. We start out by briefly reviewing the formalism behind the effective potential [38–40] before proceeding with its determination in the large-N expansion. Technical aspects of this loop calculation are collected in the Appendix.

A. Definition

The effective potential V_{eff} is defined as the generating functional of all one-particle irreducible (1PI), zero-momentum Green's functions. Following the procedures outlined in [38–40], we obtain the generating functional of all 1PI Green's functions Γ by shifting the N-component scalar field $\phi = \langle\phi\rangle + \hat{\phi}$ around a constant background field $\langle\phi\rangle$, along with integrating out the quantum fluctuations; i.e.,

$$e^{i\Gamma[\langle\phi\rangle]} = \int \mathscr{D}\hat{\phi} e^{i\int \mathrm{d}^3x[\mathcal{L}(\langle\phi\rangle+\hat{\phi})+J\hat{\phi}]}. \tag{8}$$

By construction, taking the nth functional derivative of $\Gamma[\langle\phi\rangle]$ with respect to $\langle\phi\rangle$ and setting $\langle\phi\rangle = 0$ yields the corresponding n-point 1PI Green's function. All one-point tadpoles in $\hat{\phi}$ are subtracted by the source term $J = -\delta\Gamma[\langle\phi\rangle]/\delta\langle\phi\rangle$.

Performing the path integral in (8) leads to the 1PI effective action

$$\Gamma[\langle\phi\rangle] = \int \mathrm{d}^3x[-V_{\text{eff}}(\langle\phi\rangle) + \mathcal{O}(\partial\langle\phi\rangle)], \tag{9}$$

whose zero-momentum term is given by the effective potential V_{eff}. On a practical level, $\langle\phi\rangle$ can be assumed as constant and absorbed into masses and couplings of the quantum field $\hat{\phi}$. The effective potential is then obtained via

$$\begin{aligned}
V_{\text{eff}}(\langle\phi\rangle) = V_{\text{cl}}(\langle\phi\rangle) &- \frac{i}{2}\int \frac{\mathrm{d}^3k}{(2\pi)^3}\log\left[\det i\mathscr{P}(k,\langle\phi\rangle)\right] \\
&+ \left\langle 0\middle| T\exp\left(i\int d^3x\mathcal{L}_{\text{int}}\right)\middle|0\right\rangle.
\end{aligned} \tag{10}$$

Here, V_{cl} is the classical potential appearing in the Lagrangian, $\mathscr{P}$ is the inverse propagator of the quantum field $\hat{\phi}$ and $\mathcal{L}_{\text{int}}$ is the interaction Lagrangian containing cubic and higher self interactions in $\hat{\phi}$. Diagrammatically, the tree-level term corresponds to the classical potential, the logarithmic determinant to the one-loop vacuum tadpole, and the last term comprises all two- and higher loop contributions. Equation (10) allows for a systematic computation of V_{eff}, equivalent to the standard perturbative loop expansion. In general, the action may contain several scalars, each of which has to be decomposed into a background field and one or more modes of quantum fluctuations. Equation (10) generalizes to

$$V_{\text{eff}} = V_{\text{cl}} - \frac{1}{12\pi}\sum_{\hat{\phi}} m_{\hat{\phi}}^3 + V_{\text{1PI}} \tag{11}$$

[3]We follow the convention $\phi_{\text{bare}} = \sqrt{Z_\phi}\phi$ and $\gamma_\phi = \frac{1}{2}\mathrm{d}\log Z_\phi/\mathrm{d}\log\mu$.

in three spacetime dimensions, where the second term sums over all scalar quantum fluctuations, and the third term stems from all 1PI vacuum diagrams at two loops and higher. They correspond to the second and third terms in (10).

B. Large-N limit

Now, we compute the effective potential for the theory (1) with vanishing mass and quartic coupling, i.e., $m = \lambda = 0$, at leading order (LO) in large N. We shift the scalar field $\phi = \langle\phi\rangle + \hat{\phi}$ around a constant background field $\langle\phi\rangle$, which can be rotated into a single component φ using the global symmetry transformations. The explicit construction

$$\phi(x) = (\varphi + H(x), G_1(x), \ldots, G_{N-1}(x))^\intercal \tag{12}$$

breaks the global symmetry down to $O(N-1)$, and the shifted quantum field $\hat{\phi}$ consists of a Higgs mode H as well as a $(N-1)$-component Nambu–Goldstone mode G with components labeled by G_i with $i = 1, \ldots, N-1$. The single field H does not contribute to the effective potential at LO in the large-N limit. Only interactions of the G_i are relevant, which are described by the potential

$$V_G = \frac{\eta}{6!}\varphi^6 + \frac{1}{2}\frac{\eta\varphi^4}{120}G^2 + \frac{1}{4!}\frac{\eta\varphi^2}{10}G^4 + \frac{\eta}{6!}G^6, \tag{13}$$

with $G^2 \equiv G_i G_i$. The first term represents the classical potential, and the second is a mass term for the quantum field G_i, followed by a quartic and sextic interaction. This leads to the LO effective potential

$$V_{\text{eff}}^{\text{LO}} = \frac{\eta}{6!}\varphi^6\left[1 - \frac{N}{4\pi}\sqrt{\frac{\eta}{30}}\right] + V_{\text{1PI}}^{\text{LO}}, \tag{14}$$

where the second term arises from the one-loop contribution to (11), which sums over the masses of all real scalar modes in the theory, and $V_{\text{1PI}}^{\text{LO}}$ denotes all higher loop terms. They are given by the tadpole diagrams

$V_{\text{1PI}}^{\text{LO}} =$ 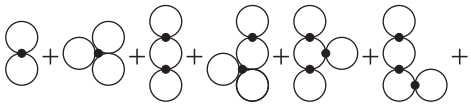 $+\ldots.$ (15)

For the effective potential to remain finite in the large-N limit, we proceed to discuss the large-N scaling of the LO contributions (15). Consider an ℓ-loop graph $\mathcal{G}$ consisting of p propagators and including n_6 sextic as well as n_4 quartic interactions. Due to being a vacuum diagram, the relation

$$p = 3n_6 + 2n_4 \tag{16}$$

holds. Moreover, the mass dimensions of the potential implies

$$[V] = 3 = 3\ell - 2p + n_4. \tag{17}$$

Each of the LO diagrams (15) fulfills

$$\ell = 1 + n_4 + 2n_6. \tag{18}$$

Overall, the leading-N contribution of the graph reads

$$\mathcal{G} \propto N^\ell \eta^{n_6+n_4-p+3\ell/2}\varphi^6 = N^\ell \eta^{1+\ell/2}\varphi^6. \tag{19}$$

Note that (19) also holds for the one-loop term in (14). Thus, the leading large-N scaling of the effective potential remains the same for all loop orders, if the sextic coupling is rescaled via

$$\bar{\eta} \equiv \frac{N^2\eta}{(4\pi)^2 5!}, \tag{20}$$

with additional factors for later convenience. This means that the effective potential is suppressed by an overall factor of N^{-2}.

Before computing the LO effective potential (14), let us address the apparent discrepancy between the leading-N contributions to the β function and the effective potential, which are captured by the rescalings (3) and (20), respectively. To be precise, $\bar{\eta} = 1/120\sqrt{N}\hat{\eta}$. It is no contradiction that both quantities require a different scaling of the coupling η to be finite but nonzero in large-N limit.

The effective potential is obtained from the finite terms of 1PI vacuum graphs. At LO in large-N, all contributions stem from the tadpole graphs displayed in (15), which warrant the rescaling (20). On the other hand, the β function is extracted from $1/\varepsilon$ poles in dimensional regularization. The tadpoles (15) neither exhibit such poles nor contribute as subgraphs to diagrams that do. In mass-independent regularization schemes, this can be readily understood: scalars can be treated as massless when computing UV poles, and tadpoles vanish altogether in this case. Even in regularization schemes where massless tadpoles do not vanish, they do not enter in the renormalization of the sextic interaction, but rather of the scalar mass and quartic operator. This is evident in cutof -schemes, where $\bar{\eta}$ does not require a counterterm; see, e.g., [16]. In consequence, leading-N contributions to the β function take the shape of (4), which are captured by the rescaling (3).

The RG evolution of $\bar{\eta}$ at $1/N$ is

$$\beta_{\bar{\eta}} = \frac{24\bar{\eta}^2 - 2\pi^2\bar{\eta}^3}{N} + \mathcal{O}(N^{-2}). \tag{21}$$

Thus, the UV fixed point still prevails

$$\bar{\eta}^* = \frac{12}{\pi^2} + \mathcal{O}(N^{-1}) \approx 1.2159 + \mathcal{O}(N^{-1}). \tag{22}$$

As before, the leading correction of (22) is already determined with two- and four-loop β functions, and its N^{-1} correction requires both six- and eight-loop RGEs. Note that (22) does not appear to be under strict perturbative control as it approaches a finite value for $N \to \infty$. This is merely an artifact of the rescaling (20); its existence is still guaranteed to all orders of the β function, as demonstrated in Sec. II.

In contrast, taking the naive limit $N \to \infty$ in (21) leads to the conclusion that the theory can be treated as conformal for all values of $\bar{\eta}$, revealing a line of fixed points that extends until it is broken by other means [21,31,41,42]. This interpretation does not actually capture the leading large-N dynamics (4) of the RG evolution. The line of fixed points is an artifact of employing a large-N rescaling, which renders the entire β function subleading, and then dropping it entirely before analysing for fixed points. In consequence, the line cannot be justified in a consistent $1/N$ expansion (21) and breaks down as soon as subleading contributions are included to the β functions [19,20,25]. Furthermore, a continuous line in $\bar{\eta}$ cannot simply emerge at "$N = \infty$" as this would mean that the theory is noninteracting due to $\eta \propto \bar{\eta}/N^2 = 0$.

In [30,32], it has been argued that the line of fixed points can be approached in dimensional continuation around $d = 3 - \varepsilon$ via a combined $N \to \infty$ and $\varepsilon \to 0$ limit. In this case, two fixed points

$$\bar{\eta}_\mp(\alpha) = \frac{6}{\pi^2}\left(1 \mp \sqrt{1 - \frac{\pi^2}{36}\alpha}\right) + \mathcal{O}(N^{-1}) \tag{23}$$

emerge [7,43] where

$$\alpha = \lim_{\substack{N\to\infty \\ \varepsilon\to 0}} \varepsilon N \quad \text{with} \quad 0 \le \alpha \le \frac{36}{\pi^2} \tag{24}$$

is a free parameter that describes how the double limit is taken. Each valid choice of α corresponds to a fixed point, forming a line that lies asymptotically below three spacetime dimensions. However, the hard limit $d = 3$ with large N stipulates $\alpha = 0$, where only the trivial $(\bar{\eta}_-(0) = 0)$ and UV fixed point $(\bar{\eta}_+(0) = \bar{\eta}^*)$ are retained.

Instead of a line of conformal fixed points, there is merely an accidental scale invariance in the LO large-N contributions to the effective potential. Once subleading terms are included, this scale invariance is broken and only recovered at the UV fixed point (22). An analogous picture should also emerge using the FRG when the expansion of the flow equation and the large-N limit are interchanged. Note, however, that consistent results beyond leading-N might require a departure from the local potential approximation.

Next, we devise a strategy to resum all LO loop diagrams (15) contributing to the effective potential. A direct summation of vacuum graphs (15) is complicated to generalize without double counting. However, all LO contributions take the form of repeated tadpole insertions and into scalar propagators. Thus, all LO terms can be resummed by introducing a dressed propagator

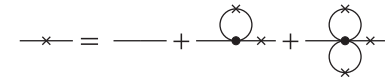

(25)

The tadpoles of (25) factorize and are finite when integrating over loop momenta. Thus, their resummation is equivalent to introducing a dynamical mass parameter M^2 of the quantum field in addition to its mass $m^2 = 1/120\eta\varphi^4$, recursively defined via a gap equation

$$M^2 = m^2 - \frac{N\eta\varphi^2 M}{240\pi} + \frac{N^2\eta M^2}{1920\pi^2}. \tag{26}$$

We find two solutions [17,44,45]

$$M_\pm = \frac{4\pi}{N}\frac{\varphi^2}{1 \pm \bar{\eta}^{-1/2}}. \tag{27}$$

It is straightforward to verify that only M_+ corresponds to a perturbative expansion of the gap equation by recursively inserting (26) into its lhs up to a finite power of m and comparing with (27) expanded as a power series in $\bar{\eta}$. On the other hand, M_- does not reproduce the perturbative expansion and is negative for small values of $\bar{\eta}$, though the sign changes for $\bar{\eta} > 1$. Whether this solution is nonperturbative or rather spurious shall be addressed later.

All leading large N, quantum corrections are resummed by inserting the dynamical mass parameter M_+ (27) in the propagator of the quantum field G_i in place of the tree-level mass. Thus, the naive expectation would be that all LO contributions to the effective potential (15) can be resummed by inserting M_+ into the one-loop term (11) of the effective potential

$$V_{\text{eff}}^{\text{LO}} \overset{?}{=} \frac{\eta}{6!}\varphi^6 - \frac{N}{12\pi}M_+^3, \tag{28}$$

and not include any explicit higher-loop diagrams. However, this approach does not reproduce the perturbative expansion of (15). The 1PI effective potential is inadequate for resummation techniques that rely on insertion of bilinear operators, such as a dynamical mass term. The ansatz (11) integrates out all tree-level bilinears and assumes that all two-loop and higher contributions are due to operators that are at least cubic in the field. To compute the effective action, the diagrams in (15) either need to be resummed without relying on the dynamical mass, or the formalism needs to be extended to keep track

of both $\langle\phi\rangle$ and bilinears $\langle\phi^2\rangle$ separately [46]. We opt for the latter option, which we will review in the next section.

C. Composite operator effective action

In this section, we review the formalism developed in [46]. For ease of notation, we will work in an example theory with a single scalar field Φ, for which we formulate an effective action $\Gamma[\phi,\chi]$ in terms of the classical field $\phi(x) \equiv \langle\Phi(x)\rangle$, but also the composite bilinear operator $\chi(x,y) \equiv \langle T\Phi(x)\Phi(y)\rangle$. To this end, the generating functional of all connected Greens functions is defined with two source terms

$$e^{iW[J,K]} = \int \mathcal{D}\Phi \exp\left\{ i \int \mathrm{d}^3x \left[\mathcal{L}(\phi(x)) + J(x)\Phi(x) + \frac{1}{2}\int \mathrm{d}^3y \Phi(x) K(x,y) \Phi(y) \right] \right\}, \tag{29}$$

which is then shifted by a double Legendre transformation

$$\Gamma[\phi,\chi] = W[J,K] - \int \mathrm{d}^3x J(x)\phi(x) - \frac{1}{2}\iint \mathrm{d}^3x\mathrm{d}^3y (\phi(x)\phi(y) + \chi(x,y)) K(x,y), \tag{30}$$

yielding the effective action of all connected, *two-particle irreducible* (2PI) Greens functions $\Gamma[\phi,\chi]$. Roughly speaking, the effective action $\Gamma[\phi,\chi]$ is obtained by shifting scalar fields around a classical background $\Phi \mapsto \Phi + \phi$ as well as all connected two-point correlators by χ before integrating out Φ. Writing the original action as $S[\phi] = \int \mathrm{d}^3x \mathcal{L}(\phi(x))$, the effective action is obtained via

$$\Gamma[\phi,\chi] = S[\phi] + \frac{i}{2}\mathrm{Tr}\left[\log\chi^{-1} + \frac{\delta^2 S}{\delta\phi^2}\chi\right] + S_{\text{2PI-int}}, \tag{31}$$

where $\mathrm{Tr}[\ldots]$ includes a spacetime integration but in general also a trace of global indices and different species of scalar fields. $S_{\text{2PI-int}}$ contains all two-particle irreducible graphs at two-loop or higher, with χ being used as a dressed propagator, and all cubic and higher order interaction vertices obtained after shifting Φ around ϕ. The one-particle irreducible effective action

$$\Gamma[\phi] = \Gamma[\phi,\chi_0] \tag{32}$$

is recovered by inserting $\chi = \chi_0$ at a stationary point of the action

$$\left.\frac{\delta\Gamma[\phi,\chi]}{\delta\chi}\right|_{\chi=\chi_0} = 0, \tag{33}$$

which corresponds to classical solutions of the path integral such as ground states. Note that the condition (33) is equivalent to a gap equation for the field Φ.

Analogously to the effective potential of the scalar field ϕ (10), the composite effective potential V_{2PI} is obtained as the generating functional of all *zero-momentum* 2PI Green's functions; i.e.,

$$\Gamma[\phi,\chi] = \int \mathrm{d}^3x [-V_{\text{2PI}}(\phi,\chi) + \mathcal{O}(\partial\phi,\partial\chi)]. \tag{34}$$

D. Leading order potential

We now apply the composite-operator formalism (31) to compute the effective potential at leading order at large N. As before, we employ the decomposition (12), which shifts ϕ around a constant background field φ. We also utilize that only the Nambu-Goldstone mode G_i gives corrections at leading order in large N and that these can be resummed into a mass parameter M for this field via (25). Thus, the formalism [46] can be condensed into a more practical shape: instead of dealing with a dressed propagator, which also resums loop corrections that are explicitly momentum dependent, it is sufficient to keep track of a dynamical mass parameter M. Concretely,

$$\chi^G_{ij}(x,y) = \langle T G_i(x) G_j(y)\rangle = \delta_{ij}\int \frac{\mathrm{d}^d p}{(2\pi)^d}\frac{e^{-ip(x-y)}}{p^2 - M^2} \tag{35}$$

is a suitable ansatz for the dressed propagator.

Using the vertex rules stemming from (13), we compute (31) and collect all nonderivative terms of the 2PI effective action in an effective potential V_{2PI}. The one-loop corrections, dimensionally regularized in $d = 3 - 2\varepsilon$, read

$$\begin{aligned} S[\phi]|_\varphi &= -\frac{\eta}{6!}\varphi^6 \int \mathrm{d}^3x, \\ \mathrm{Tr}[\log\chi^{-1}]|_\varphi &= (N-1)\int \frac{\mathrm{d}^d p}{(2\pi)^d}\log(p^2 - M^2)\int \mathrm{d}^3x, \\ \mathrm{Tr}\left[\frac{\delta^2 S}{\delta\phi^2}\chi\right]\Big|_\varphi &= (N-1)\int \frac{\mathrm{d}^d p}{(2\pi)^d}\frac{p^2 - \frac{1}{120}\eta\varphi^4}{p^2 - M^2}\int \mathrm{d}^3x, \end{aligned} \tag{36}$$

when evaluated at $\phi(x) = \varphi$. Thus, we obtain

$$V_{\text{2PI}} = \frac{\eta}{6!}\varphi^6 - \frac{NM^3}{12\pi} - \frac{NM}{8\pi}\left(\frac{\eta\varphi^4}{120} - M^2\right) + V_{\text{2PI-int}}, \tag{37}$$

where the first three terms correspond to the ones of (31) in the same order. The last term $V_{\text{2PI-int}}$ marks the sum of all 2PI vacuum graphs with the dressed propagator (35). It reads

$V_{\text{2PI-int}} =$ 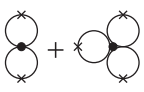 $= \frac{N^2\eta\varphi^2M^2}{3840\pi^2} - \frac{N^3\eta M^3}{46080\pi^3}.$ (38)

Overall, we find

$$V_{\rm 2PI}(\varphi, M) = \frac{\eta}{6!}\left(\varphi^2 - \frac{NM}{4\pi}\right)^3 + \frac{NM^3}{24\pi}, \tag{39}$$

at leading order in large N. Note (39) assumes $M \geq 0$ as M should be taken as the absolute value of the mass, since it stems from tadpole integrals

$$\int \frac{\mathrm{d}^3 p}{(2\pi)^3}\frac{1}{p^2 - M^2} = \frac{i|M|}{4\pi}. \tag{40}$$

The result (39) has also been obtained using a variational method in the literature [19,20,22]. The 1PI effective potential is retrieved at stationary points in M; i.e.,

$$\frac{\partial V_{\rm 2PI}}{\partial M} = 0, \tag{41}$$

which yields the gap equation (26), and we recover the solutions $M_\pm$ (27). They are extrema of $V_{\rm 2PI}$ as depicted in Fig. 2. The perturbative solution M_+ indeed corresponds to a stable local minimum of the effective potential. The other solution M_- is invalid for $\bar{\eta} < 1$ as $M_- < 0$ and has a singularity for $\bar{\eta} = 1$. For $\bar{\eta} > 1$, M_- is a maximum of $V_{\rm 2PI}(M)$, while M_+ is a minimum [45]. Thus, M_+ and M_- represent distinct vacua of the effective potential, though only M_+ corresponds to the ground state as the effective potential is deeper than for M_-. However, both solutions $M_\pm$ become degenerate at $\varphi = 0$.

Inserting M_+ into (39) yields the LO 1PI potential

$$V_{\rm eff} = \frac{(4\pi)^2\varphi^6}{N^2}\frac{\bar{\eta}}{6(1+\sqrt{\bar{\eta}})^2} + \mathcal{O}(N^{-3}). \tag{42}$$

The effective potential typically contains higher-dimensional operators, which are summed up as logarithms $\log\varphi^2/\mu$, where μ is the renormalization scale. Such contributions are subleading in the large-N expansion and hence absent in (42). This can be readily understood since the effective potential is overall RG invariant, so the explicit RG dependence in terms $\log\varphi^2/\mu$ needs to be canceled by the running of $\bar{\eta}$ and φ, which are both subleading. Furthermore, (42) naively implies that the effective potential is always stable for any value of the coupling $\bar{\eta}$. In particular, that would render the UV fixed point (22) valid. However, it is commonly believed that the nonperturbative BMB phenomenon impedes this conclusion. We will turn to this phenomenon in a later section. Next, we extend the effective potential to order $\propto 1/N^3$.

E. Next-to-leading order potential

We are now in a position to compute the next-to-leading order (NLO), i.e., $1/N^3$, corrections to the effective potential. To this end, we must also include interactions of the Higgs mode H with the potential (13)

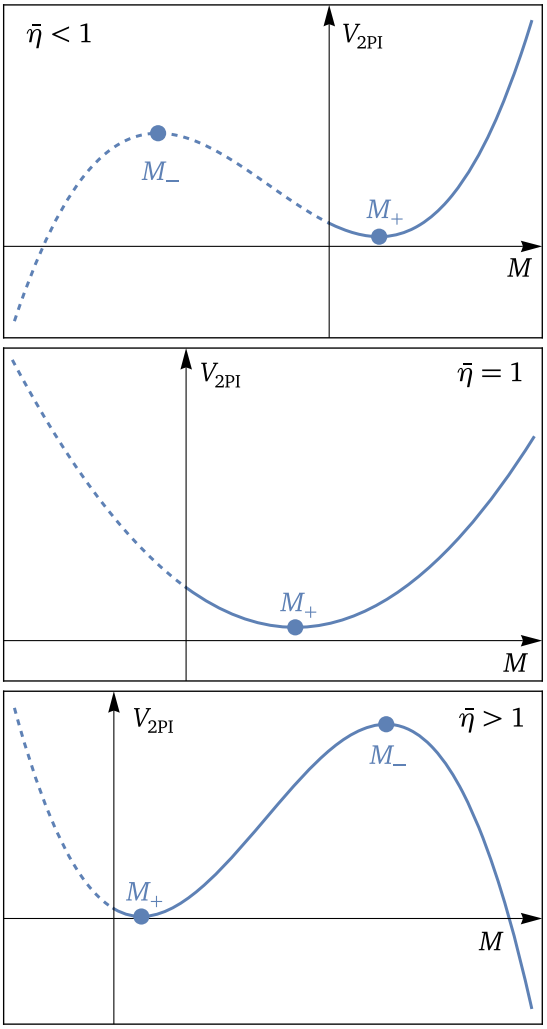

FIG. 2. $V_{\rm 2PI}(M)$ for a fixed value $\varphi > 0$ and $\bar{\eta} < 1$ (top panel), $\bar{\eta} = 1$ (middle panel), and $\bar{\eta} > 1$ (bottom panel). Only values $M \geq 0$ (solid blue line) are valid arguments of $V_{\rm 2PI}(M)$, while $V_{\rm 2PI}(M < 0)$ (dashed blue line) is only drawn for convenience. The extrema $M_\pm$ (27) are indicated by blue dots. The minimum M_+ always exists, while the maximum M_- is only found for $\bar{\eta} > 1$. At $\varphi = 0$, both points are shrunk together at $M_\pm = 0$, and $V_{\rm 2PI}$ becomes flat for $\bar{\eta} = 1$. The plot is adapted from [45].

$$\begin{aligned} V = V_G &+ \frac{1}{2}\frac{\eta\varphi^4}{24}H^2 + \frac{1}{3!}\frac{\eta\varphi^3}{6}H^3 + \frac{1}{4!}\frac{\eta\varphi^2}{2}H^4 \\ &+ \frac{1}{5!}\eta\varphi H^5 + \frac{1}{6!}\eta H^6 + \frac{1}{2}\frac{\eta\varphi^3}{30}G^2H \\ &+ \frac{1}{4}\frac{\eta\varphi^2}{10}G^2H^2 + \frac{1}{12}\frac{\eta\varphi}{5}G^2H^3 + \frac{1}{48}\frac{\eta}{5}G^2H^4 \\ &+ \frac{1}{4!}\frac{\eta\varphi}{5}G^4H + \frac{1}{48}\frac{\eta}{5}G^4H^2, \end{aligned} \tag{43}$$

where $G^2 \equiv G_iG_i$, and the tadpole term $\propto H$ was removed by the source term in the effective potential. In particular,

the Higgs mode exhibits a mass $\tilde{m}^2 = \eta\varphi^4/24$ and gives rise to multiple interactions $\propto \eta$.

We shall now lay out a strategy to compute the effective potential at NLO. At LO, we adopted a practical version of the 2PI formalism [46] to properly resum tadpole graphs into a mass parameter, cf. (25). This was possible because all LO contributions factorize. At NLO, this is not the case: Dressed propagators for both G_i and H include loop corrections that depend explicitly on the momentum routed through the propagator. As a result, dynamical mass parameters cannot resum all NLO corrections. Therefore, it is not possible to define V_{2PI} in terms of dynamical mass parameters alone at NLO. Nevertheless, we will retain dynamical mass parameters in order to resum all tadpole-type contributions. Other contributions to V_{eff} are computed explicitly. In this sense, we employ propagators χ^G_{ij} and χ^H for the fields G_i and H that are *half-dressed* by dynamical mass parameters M and $\tilde{M}$, respectively. Explicitly, for χ^G_{ij}, we use the ansatz (35), while the Higgs propagator reads

$$\chi^H(x,y) = \langle TH(x)H(y)\rangle = \int \frac{\mathrm{d}^d p}{(2\pi)^d}\frac{e^{-ip(x-y)}}{p^2-\tilde{M}^2}. \tag{44}$$

A careful analysis of all possible Feynman graphs reveals that all LO and NLO contributions to the effective potential can be decomposed as

$$V^{\mathrm{NLO}}_{\mathrm{eff}} = \frac{\eta\varphi^6}{6!} + V_{\mathrm{1L}} + V_{\mathrm{tad}} + V_{\mathrm{ring}} + V_{\mathrm{ct}}. \tag{45}$$

The first term is the classical potential, while $V_{\mathrm{1L,tad,ring,ct}}$ are all quantum corrections from integrating out both Goldstone and Higgs modes. The V_{1L} and V_{tad} contain all one-loop and 2PI tadpole diagrams, yielding both contributions at LO and NLO. V_{ring} contains additional diagrams that are purely NLO, while V_{ct} are LO diagrams with counterterm insertions that render them NLO. We now compute (45) piece by piece.

V_{1L} is obtained by applying (36) for both Goldstone and Higgs mode, yielding

$$\begin{aligned} V_{\mathrm{1L}} = &-\frac{(N-1)M^3}{12\pi} - \frac{(N-1)M}{8\pi}\left(\frac{\eta\varphi^4}{120} - M^2\right) \\ &-\frac{\tilde{M}^3}{12\pi} - \frac{\tilde{M}}{8\pi}\left(\frac{\eta\varphi^4}{24} - \tilde{M}^2\right). \end{aligned} \tag{46}$$

The tadpole contributions are

$V_{\mathrm{tad}} =$ 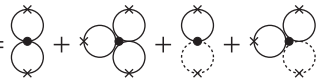

$$= \frac{\bar{\eta}}{2}(\varphi M)^2 - \frac{N+3}{24\pi}\bar{\eta}M^3 + \frac{3\bar{\eta}}{N}\varphi^2\tilde{M}M - \frac{\bar{\eta}}{8\pi}\tilde{M}M^2 \tag{47}$$

when expanded up to NLO. Here, the dashed lines represent propagators of the Higgs, the solid lines correspond to the Goldstone mode, and crosses denote dressed propagators in either case. This leads to the intermediate result

$$\begin{aligned} V_{\mathrm{1L}} + V_{\mathrm{tad}} = &\frac{(N-1)M^3}{24\pi} + \frac{8\pi^2\bar{\eta}}{3N^2}\left(\varphi^2 - \frac{MN}{4\pi}\right)^3 \\ &+ \frac{\tilde{M}^3}{24\pi} - \frac{2\pi\bar{\eta}}{N^2}\left(\varphi^2 - \frac{MN}{4\pi}\right)^2(\tilde{M}+M) \\ &+ \frac{4\pi\bar{\eta}}{N^2}\left(\varphi^2 - \frac{MN}{4\pi}\right)\varphi^2(M-2\tilde{M}). \end{aligned} \tag{48}$$

Tadpoles are resummed when inserting the $\tilde{M}$ at the stationary value

$$\frac{\partial(V_{\mathrm{1L}} + V_{\mathrm{tad}})}{\partial\tilde{M}} = 0, \tag{49}$$

which yields the gap equation

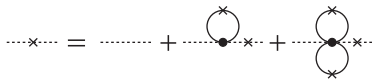

(50)

Computing (50) explicitly, we obtain

$$\tilde{M}^2 = \frac{\eta}{24}\varphi^4 - \frac{N\eta M\varphi^2}{80\pi} + \frac{N^2\eta M^2}{1920\pi^2}. \tag{51}$$

Inserting the leading-order mass $M = M_+$ (27), this simplifies to

$$\tilde{M} = \frac{4\pi\varphi^2}{N}\frac{\sqrt{5+4\sqrt{\bar{\eta}}}}{1+\bar{\eta}^{-1/2}}. \tag{52}$$

Similarly, computing the stationary value of M via the condition

$$\frac{\partial(V_{\mathrm{1L}} + V_{\mathrm{tad}})}{\partial M} = 0 \tag{53}$$

yields the NLO corrections δM to Goldstone mass; i.e., $M = M_+ + \delta M$. However, the value of δM does not contribute to the NLO effective potential as such a term would read

$$\delta M \frac{\partial (V_{1L} + V_{tad})}{\partial M}\bigg|_{M=M_+} = 0. \tag{54}$$

Now we consider the correction V_{ring} in (45). It is a sum of two families of ring diagrams; i.e.,

$$V_{ring} = \sum_{n=2}^{\infty} R_n + \sum_{n=1}^{\infty} \tilde{R}_n. \tag{55}$$

The ring diagrams R_n and $\tilde{R}_n$ each consist of subgraphs of the sort

(56)

The first family, R_n, only involves the Goldstone and consists of n pieces

$R_n =$

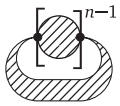

(57)

such that the connection between each piece is a quartic or sextic vertex. For instance,

$R_{2,3,4,5,\ldots} =$

(58)

We relegate the details regarding the computations to the Appendix and present the results here. The first two diagrams R_2 and R_3 are UV divergent. We obtain

$$\begin{aligned} R_2 = & \frac{4\pi\bar{\eta}^2 M(\varphi^2 - \frac{NM}{4\pi})^2}{N^2\varepsilon} \\ & - \frac{4\bar{\eta}^2 M^2(\varphi^2 - \frac{NM}{4\pi})}{N}\left[1 - \log 2 - \log\frac{M}{\mu}\right] \\ & + \frac{8\pi\bar{\eta}^2 M(\varphi^2 - \frac{NM}{4\pi})^2}{N^2}\left[4 - 5\log 2 - 3\log\frac{M}{\mu}\right], \end{aligned} \tag{59}$$

and

$$\begin{aligned} R_3 = & \frac{2\pi^4\bar{\eta}^3(\varphi^2 - \frac{NM}{4\pi})^3}{3N^3\varepsilon} \\ & + \frac{4\pi^4\bar{\eta}^3(\varphi^2 - \frac{NM}{4\pi})^3}{3N^3}\left[1 - \frac{42\zeta_3}{\pi^2} - 2\log\frac{2M^2}{\mu^2}\right] \\ & - \frac{\pi^3\bar{\eta}^3 M(\varphi^2 - \frac{NM}{4\pi})^2}{N^2}\left[1 - \log 2 - \log\frac{M}{\mu}\right]. \end{aligned} \tag{60}$$

For $n \geq 4$, the R_n are finite and read

$$R_n = -\frac{2M^3}{\pi^2 n}\left[\bar{\eta}\left(1 - \frac{4\pi\varphi^2}{NM}\right)\right]^n \int_0^\infty \frac{\arctan^n(z)}{z^{n-2}} \mathrm{d}z. \tag{61}$$

Diagram summation and momentum integration may be exchanged if the results are convergent, and we obtain

$$\sum_{n=4}^{\infty} R_n = \frac{2M^3}{\pi^2} f\left(\bar{\eta}\left(1 - \frac{4\pi\varphi^2}{NM}\right)\right), \tag{62}$$

with the function

$$\begin{aligned} f(x) = \int_0^\infty \mathrm{d}z \Big[& xz\,\arctan(z) + \frac{1}{2}x^2\arctan^2 z \\ & \frac{x^3\arctan^3 z}{3z} + z^2\log\left(1 - \frac{x\arctan z}{z}\right)\Big], \end{aligned} \tag{63}$$

which can be evaluated numerically within its radius of convergence $x \leq 1$. The second family $\tilde{R}_n$ consists of several sequences of subgraphs (56); i.e.,

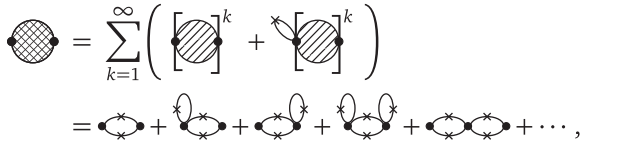

(64)

such that they are connected by n lines of the Higgs field

$\tilde{R}_n =$

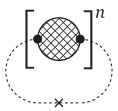

. (65)

In the following, we first consider the diagrams belonging to $\tilde{R}_1$, which contain a single Higgs line. We divide them into a subfamily $\tilde{R}_{1,l}$, where l labels the number of insertions of the blob (56)

$\tilde{R}_{1,l} =$

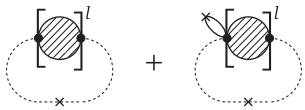

. (66)

Only the graphs $\tilde{R}_{1,1}$ are UV divergent

$$\tilde{R}_{1,1} = \quad + \quad + \quad$$
$$= -\frac{16\pi^2\bar{\eta}^2\varphi^2\left(\varphi^2-\frac{NM}{4\pi}\right)^2}{N^3\varepsilon} - \frac{64\pi^2\bar{\eta}^2\varphi^2\left(\varphi^2-\frac{NM}{4\pi}\right)^2}{N^3}\left[\frac{1}{2}-\log\left(\frac{2M+\tilde{M}}{\mu}\right)\right] + \frac{16\pi\bar{\eta}^2M\varphi^2\left(\varphi^2-\frac{NM}{4\pi}\right)}{N^2}\left[1-\log 2-\log\frac{M}{\mu}\right], \tag{67}$$

while the remaining ones are finite and simply read

$$\tilde{R}_{1,l} = -\frac{8M^2\varphi^2}{\pi N}\left[\bar{\eta}\left(1-\frac{4\pi\varphi^2}{NM}\right)\right]^{l+1}\int_0^\infty \frac{\arctan^l(z)\mathrm{d}z}{z^{l-2}(z^2+\frac{\tilde{M}^2}{4M^2})}, \tag{68}$$

for $l \geq 2$. Returning to the superfamily $\tilde{R}_n$, all graphs $n \geq 2$ are UV finite as well. Inserting (27) and (52), they can be written as

$$\tilde{R}_n = -\frac{256\pi\bar{\eta}^{3/2}\varphi^6}{(1+\sqrt{\bar{\eta}})^3N^3} \times \int_0^\infty \mathrm{d}z\frac{z^2}{n}\left[\frac{2\sqrt{\bar{\eta}}(1+\sqrt{\bar{\eta}})\arctan z}{(4z^2+5+4\sqrt{\bar{\eta}})(\sqrt{\bar{\eta}}\arctan z+z)}\right]^n. \tag{69}$$

Summing the results of (61), (68), and (69) gives

$$\sum_{n=4}^\infty R_n + \sum_{n=2}^\infty(\tilde{R}_{1,n}+\tilde{R}_n) = \frac{128\pi\bar{\eta}^{3/2}\varphi^6}{(1+\sqrt{\bar{\eta}})^3N^3}F(\sqrt{\bar{\eta}}), \tag{70}$$

where $F(\sqrt{\bar{\eta}})$ is a function that can be evaluated numerically

$$F(x) = \int_0^\infty \mathrm{d}z\left[-\frac{xz(1+4z^2)\arctan z}{5+4x+4z^2}+\frac{x^2}{2}\arctan^2 z - \frac{x^3}{3z}\arctan^3 z - z^2\log\left(1+\frac{x}{z}\arctan z\right) + 2z^2\log\left(1+\frac{x(3+2x+4z^2)}{z(5+4x+4z^2)}\arctan z\right)\right]. \tag{71}$$

Finally, all UV divergencies arising at NLO are subtracted minimally by computing LO vacuum graphs with counterterm insertions. The scalar field variable φ has a counterterm $\delta\varphi = \mathcal{O}(N^{-2})$, which only contributes to the effective potential at N^{2}LO in large N. On the other hand, the sextic coupling is renormalized via $\bar{\eta} \mapsto \bar{\eta} + \delta\bar{\eta}/\varepsilon$ with

$$\delta\bar{\eta} = \frac{6\bar{\eta}^2}{N}\left(1-\frac{\pi^2}{24}\bar{\eta}\right) + \mathcal{O}(N^{-2}), \tag{72}$$

which includes two- and four-loop contributions [7], while higher loops and higher poles are of order $\mathcal{O}(N^{-2})$. This implies a counterterm from the tree-level potential $\delta\eta\varphi^6/(6!\varepsilon)$ as well as mass, quartic, and sextic couplings to G_i, marked as $\otimes$ below. The counterterm potential reads

$$V_{\mathrm{ct}} = \frac{(4\pi)^2\varphi^6}{6}\frac{\delta\bar{\eta}}{\varepsilon N^2} + \quad + \quad + \quad$$
$$= \frac{(4\pi)^2}{6}\left(\varphi^2-\frac{NM}{4\pi}\right)^3\frac{\delta\bar{\eta}}{\varepsilon N^2} - \frac{4\pi\delta\bar{\eta}M}{N}\left(\varphi^2-\frac{NM}{4\pi}\right)^2\left(1-\log 2-\log\frac{M}{\mu}\right). \tag{73}$$

The expression (73) exactly subtracts the $1/\varepsilon$ poles in the UV divergent ring diagrams (59), (60), and (67). The finite term of (73) stems from the product of the counterterm and the $\mathcal{O}(\varepsilon)$ contributions of the diagrams. The logarithmic terms $\log\mu$ in (59), (60), (67), and (73) exactly cancel the RG running of (42) as expected.

Overall, the effective potential explicitly depends on the renormalization scale μ at NLO, which signals the breaking of scale invariance by quantum fluctuations. As the potential is overall invariant under a renormalization group transformation, we choose to relate its scale to the field value

$$\mu = \frac{4\pi}{N}\varphi^2. \tag{74}$$

This choice resums higher order operators, usually contained in logarithmic terms $\log\varphi^2/\mu$ into the coupling $\bar{\eta}$. In consequence, evolving the effective potential to a different field value φ involves an RG transformation of $\bar{\eta}(4\pi\varphi^2/N)$. Due to (21) being positive until the UV fixed point, studying the potential at higher values of $\bar{\eta}(4\pi\varphi^2/N)$ is surrogate to evaluating $V_{\mathrm{eff}}/\varphi^6$ at larger field values φ.

Thus, we obtain the effective potential at NLO

$$V_{\mathrm{eff}} = \frac{(4\pi)^2\varphi^6}{6N^2}\frac{\bar{\eta}}{(1+\sqrt{\bar{\eta}})^2} + \frac{(4\pi)^2\varphi^6}{N^3}\frac{\bar{\eta}^{3/2}}{(1+\sqrt{\bar{\eta}})^3}\left[+\frac{1}{3}-\sqrt{\bar{\eta}} - \frac{1}{3}(5+4\sqrt{\bar{\eta}})^{3/2} - \frac{7}{2}\zeta_3\bar{\eta}^{3/2} + 4\bar{\eta}(1-2\log 2) + \frac{\pi^2}{12}\bar{\eta}^{3/2}(1-\log 2) - 4\sqrt{\bar{\eta}}\left(1-\frac{\pi^2}{12}\bar{\eta}\right)\log\left(1+\frac{1}{\sqrt{\bar{\eta}}}\right) + 4\sqrt{\bar{\eta}}(1+\sqrt{\bar{\eta}})\log\left(2+\sqrt{5+4\sqrt{\bar{\eta}}}\right) + \frac{8}{\pi}F(\sqrt{\bar{\eta}})\right] + \mathcal{O}(N^{-4}), \tag{75}$$

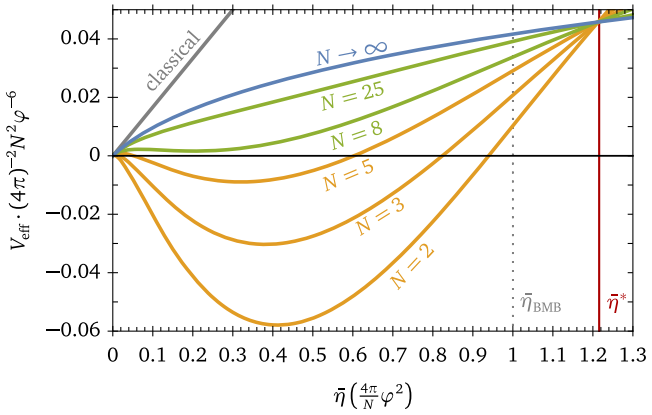

FIG. 3. Sextic term of the classical (solid gray) and next-to-leading order effective potential (75) as a function of the rescaled sextic coupling as a function of $\bar{\eta}$, evaluated at the renormalization scale $\mu = 4\pi\varphi^2/N$, for various choices of N. The limit $N \to \infty$ (blue) singles out the LO effective potential (42), which has a smaller but stable sextic coupling compared to the classical case (solid gray). With decreasing N, the potential remains stable (green) until it turns unstable at integer values $N < 8$ (yellow). However, the large-N expansion might not be reliable in this case. The BMB end point $\bar{\eta}_{\rm BMB} = 1$ (gray dashed) and Pisarski's UV fixed point (22) $\bar{\eta}^* \approx 12/\pi^2$ (red) are also shown.

where $F(\sqrt{\bar{\eta}})$ is defined in (71). Equation (75) is one of the main results of this work and also displayed in Fig. 3. For integer values $N \geq 8$, the potential is stable in the sense that it is both bounded from below and that $\varphi = 0$ is an absolute minimum. At $N < 8$, the potential is still bounded from below but develops a deeper minimum $\varphi_{\rm min} \neq 0$, hinting at spontaneous symmetry breaking. However, as (75) has been obtained in a large-N expansion, the prediction might not be reliable in this case.

The effective potential can be extended naively to Pisarski's UV fixed point $\bar{\eta}^* \approx 12/\pi^2$ (22), marked red in Fig. 3. All curves appear to be converging at this point as the NLO corrections are numerically small. While the UV fixed point is stable for sufficient large N, it has been argued that an instability occurs through the nonperturbative BMB phenomenon already at $\bar{\eta}_{\rm BMB} = 1$ [22], shown as gray dotted line in Fig. 3. We will turn toward this effect in the next section.

IV. BARDEEN-MOSHE-BANDER PHENOMENON

The BMB phenomenon [22] is a nonperturbative effect that breaks the scale invariance spontaneously through dimensional transmutation at sextic coupling values

$$\bar{\eta}_{\rm BMB} = 1. \tag{76}$$

This terminates the line of accidental scale invariance at leading order large N. Moreover, the proper UV fixed point (22) lies in the affected parameter region $\bar{\eta}^* > \bar{\eta}_{\rm BMB}$. The spontaneous breaking of scale invariance at the BMB point gives rise to a massless Nambu-Goldstone boson, the *dilaton* [22]. In the following, we review the BMB phenomenon at LO and extend its analysis to NLO in the $1/N$ expansion.

A. Leading order

Capturing the onset of the BMB is challenging in perturbation theory and especially dimensional regularization. Nevertheless, the generation of a dynamical mass $\mathscr{M}$ by quantum effects of the initially massless field ϕ can be understood from a gap equation

(77)

which encodes the resummation of all leading large-N contributions to the two-point function $\langle T\phi_i(x)\phi_j(y)\rangle$. Here, the uncrossed lines denote the massless propagators of ϕ, while the crossed ones represent dressed ones with a putative mass $\mathscr{M}$. This gap equation yields a self-consistency condition

$$\mathscr{M}^2 = \bar{\eta}\mathscr{M}^2, \tag{78}$$

which for $\bar{\eta} < \bar{\eta}_{\rm BMB}$ has only the solution $\mathscr{M} = 0$. However, for $\bar{\eta} = \bar{\eta}_{\rm BMB}$, the condition is also valid for any $\mathscr{M} \neq 0$, and a dynamical mass is generated at loop level. This leads to the formation a scalar condensate as evident from the two-point correlator

$$\langle T\phi_k(x)\phi_k(x)\rangle = \int \frac{\mathrm{d}^3k}{(2\pi)^3}\frac{iN}{k^2 - \mathscr{M}^2} = -\frac{N|\mathscr{M}|}{4\pi}, \tag{79}$$

while the global symmetry remains unbroken as $\langle\phi\rangle = 0$. Accounting for the formation of a condensate by shifting ϕ^2 around $\langle\phi^2\rangle$ yields a *trivial* gap equation

$$\mathscr{M}^2 = \bar{\eta}\mathscr{M}^2 + \frac{\eta}{120}\langle\phi^2\rangle^2 - \frac{N\eta}{240\pi}\mathscr{M}\langle\phi^2\rangle + \frac{N^2\eta}{1920\pi^2}\mathscr{M}^2, \tag{80}$$

as the last three terms cancel against each other.

The actual value of the condensate $\langle\phi^2\rangle$ or equivalent the dynamical mass scale $\mathscr{M}$ are determined by minimising the effective potential. To this end, we return to the 2PI potential $V_{\rm 2PI}(\varphi, M)$ (39). In Sec. III, we used this formalism as a vehicle to obtain the effective potenital $V_{\rm eff}(\varphi) = V_{\rm 2PI}(\varphi, M_+(\varphi))$ by inserting the minimum $M_+(\varphi)$; see (27). Here, we retain $V_{\rm 2PI}(\varphi, M)$, thus treating the field φ and the Goldstone dynamical mass M as independent quantities. This allows us to identify a different set of vacua.

The potential $V_{2\mathrm{PI}}$ (39) is shown in Fig. 2 with various values of $\bar{\eta}$ and fixed φ. For $\bar{\eta} < 1$, there is a minimum $\varphi = M = 0$, which is bounded from below and hence a stable ground state. At $\bar{\eta} = 1$, the minimum turns into a saddle point as the potential becomes flat in the direction of M. This is most obvious when projecting $V_{2\mathrm{PI}}$ onto the section $\varphi = 0$, which yields the expression

$$V_{2\mathrm{PI}}(0, M) = \frac{NM^3}{24\pi}(1 - \bar{\eta}), \tag{81}$$

which was also obtained in [26] and is displayed in Fig. 4. At $\bar{\eta} = 1$, (81) is flat, and any value of $M = \mathscr{M}$ is a valid ground state into which the system can transition, dynamically generating a scale $\mathscr{M}$ and thus breaking scale invariance. As the scale is arbitrary, we were unable to determine a fixed value in (77). The composite field

$$D(x) = \frac{1}{N}\phi_i(x)\phi_i(x) \tag{82}$$

acts as a dilaton mode that shifts the ground state to different values of $\mathscr{M}$ and is massless at the BMB due to the flatness of the 2PI potential (81). The masslessness can be seen explicitly from the LO dilaton propagator [22] in the $O(N)$ symmetric theory

$$\begin{aligned}\langle 0|D(p)D(-p)|0\rangle &= \sum_{n=0}^{\infty} \\ &= \frac{16\pi\bar{\eta}\mathscr{M}}{N\left[1 - \bar{\eta}\frac{2\mathscr{M}}{p}\arctan\frac{p}{2\mathscr{M}}\right]} \\ &= \frac{192\pi}{N}\frac{\mathscr{M}^3}{p^2 + m_D^2} + \mathcal{O}(p^4)\end{aligned} \tag{83}$$

with Euclidean momentum p. We read off the dilaton mass

$$m_D^2 = 12\left(\frac{1 - \bar{\eta}}{\bar{\eta}}\right)\mathscr{M}^2, \tag{84}$$

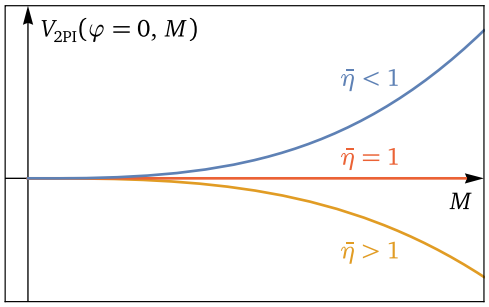

FIG. 4. Leading-order 2PI potential (81) at $\varphi = 0$ and as a function of M. For $\bar{\eta} < 1$, the potential is bounded from below and has a minimum at $M = 0$, while it is unstable for $\bar{\eta} > 1$. At $\bar{\eta} = 1$, $V_{2\mathrm{PI}}(0, M)$ is flat, and the BMB phenomenon occurs.

which indeed vanishes at $\bar{\eta} = 1$. The effective potential at the BMB point, i.e.,

$$V_{\mathrm{eff}} = \frac{1}{2}\mathscr{M}^2\varphi^2 - \frac{2\pi}{N}\mathscr{M}\varphi^4 + \frac{8\pi^2}{3N^2}\varphi^6, \tag{85}$$

has a stable ground state at $\varphi = 0$. Thus, the vacua for each value $M = \mathscr{M}$ are all degenerate. Moreover, the potential is bounded from below. This is in agreement with the FRG results [21], though the exact shape of the potential differs. This is to be expected as this detail appears to be scheme dependent already within the FRG [21].

At $\bar{\eta} > 1$, the former ground state $M = \varphi = 0$ becomes a saddle point unstable in the M direction, and the potential is not bounded from below. In the next section, we will find that this is not a sign of sickness but is merely an artifact of the LO approximation.

We close our LO discussion by pointing out that each point of $\bar{\eta}$ corresponds to a separate theory since there is no RG evolution. Thus, there is no transition from a stable $(\bar{\eta} < 1)$ to an unstable regime $(\bar{\eta} \geq 1)$. In particular, while the true UV fixed point (22) lies in the unstable regime, one cannot determine whether the BMB phenomenon impedes the RG evolution toward this fixed point at LO in large N. To do so, next-to-leading accuracy is required.

B. Next-to-leading order

Now, we investigate the BMB phenomenon at NLO in the large-N expansion by computing corrections to $V_{2\mathrm{PI}}$ (81). For simplicity, we work at the field minimum $\varphi = 0$ where the BMB instability occurs. This restores the full $O(N)$ symmetry, and we can treat all components of ϕ_k on equal footing. In general, the 2PI potential $V_{2\mathrm{PI}}$ is a functional of the dressed propagator χ_{kl} with $k, l = 1, \ldots, N$. Both of them can be expanded in the large-N limit

$$V_{2\mathrm{PI}} = V_{2\mathrm{PI}}^{\mathrm{LO}}[\chi^{\mathrm{LO}}] + V_{2\mathrm{PI}}^{\mathrm{NLO}}[\chi^{\mathrm{LO}}] + \mathrm{Tr}\left[\frac{\delta V_{2\mathrm{PI}}^{\mathrm{LO}}[\chi^{\mathrm{LO}}]}{\delta\chi^{\mathrm{LO}}}\chi^{\mathrm{NLO}}\right], \tag{86}$$

where $\mathrm{Tr}[\ldots]$ is understood as a combined summation of indices and integration of momenta. Starting from $V_{2\mathrm{PI}}$, the effective potential is obtained by inserting the stationary value of χ

$$0 = \frac{\delta V_{2\mathrm{PI}}[\chi]}{\delta\chi} = \frac{\delta V_{2\mathrm{PI}}^{\mathrm{LO}}[\chi^{\mathrm{LO}}]}{\delta\chi^{\mathrm{LO}}} + \mathcal{O}(\mathrm{NLO}), \tag{87}$$

which suggests that the third term in (86) is actually of order $\mathrm{N^2LO}$. Inserting the LO propagator

$$\chi_{kl}^{\mathrm{LO}}(p) = \frac{i\delta_{kl}}{p^2 - \mathscr{M}^2} \tag{88}$$

into the 2PI potential yields an effective potential $V_{\mathscr{M}}$ for the mass parameter $\mathscr{M}$. Explicitly, we obtain

$$V_{\mathscr{M}} = \frac{N\mathscr{M}^3}{24\pi} + \text{⊗} + \text{⊗} + \sum_{n=2}^{\infty} R_n \Big|_{\substack{\varphi=0 \\ M=\mathscr{M}}}, \tag{89}$$

where ⊗ marks the insertion of a counterterm (72), and the last terms have been computed in (59), (60), and (61). Putting all pieces together, we arrive at the potential

$$\begin{aligned} V_{\mathscr{M}} = \frac{N\mathscr{M}^3(1-\bar{\eta})}{24\pi} + \frac{\mathscr{M}^3}{24\pi}\Bigg[& -6\bar{\eta} \\ & + 12\bar{\eta}^2\left(3 - 4\log 2 - 2\log\frac{\mathscr{M}}{\mu}\right) + 21\zeta_3\bar{\eta}^3 \\ & - \frac{\pi^2\bar{\eta}^3}{2}\left(1 - 2\log 2 - 4\log\frac{\mathscr{M}}{\mu}\right) + \frac{48}{\pi}f(\bar{\eta})\Bigg], \end{aligned} \tag{90}$$

where $f(x)$ is given in (63). For the sake of discussion, we write it in the compact shape

$$V_{\mathscr{M}} = \mathscr{M}^3\left[c_0(\bar{\eta}) + c_1(\bar{\eta})\log\frac{\mathscr{M}}{\mu}\right]. \tag{91}$$

At LO, the logarithmic term is absent, i.e., $c_1 = 0$, such that the BMB phenomenon occurs when $c_0(\bar{\eta}_{\text{BMB}}) = 0$, where the minimum at $\mathscr{M} = 0$ is lifted. This yields $\bar{\eta}_{\text{BMB}} = 1$ and renders $V_{\mathscr{M}}$ exactly flat at the BMB point. At NLO, c_0 obtains corrections, but still has a zero $c_0(\bar{\eta}_0) = 0$ at

$$\begin{aligned} \bar{\eta}_0 &= 1 + \frac{\pi^2}{2N}(2\log 2 - 1) + \frac{48}{\pi N}f(1) \\ &\quad + \frac{3(10 + 7\zeta_3 - 16\log 2)}{N} + \mathcal{O}(N^{-2}) \\ &\approx 1 + \frac{9.0584}{N} + \mathcal{O}(N^{-2}). \end{aligned} \tag{92}$$

However, $\bar{\eta}_0$ is not simply the generalization of $\bar{\eta}_{\text{BMB}}$ at NLO. The stability of (91) around the ground state $\mathscr{M} = 0$ does not hinge on $c_0(\bar{\eta})$ but rather on the sign of $c_1(\bar{\eta})$, as depicted schematically in Fig. 5. Concretely, because $\log \mathscr{M}/\mu \to -\infty$ as $\mathscr{M} \to 0$, the ground state is stable for $c_1 < 0$. As evident from (90), the coefficient is related to the β function

$$c_1(\bar{\eta}) = -\beta_{\bar{\eta}} < 0, \tag{93}$$

for all $\bar{\eta} < \bar{\eta}^*$, cf. (21). This suggests that $\mathscr{M} = 0$ remains a minimum of $V_{\mathscr{M}}$, and there is no breaking of scale invariance for $0 \le \bar{\eta} \le \bar{\eta}^*$; i.e., the UV fixed point (22) exists. The appearance of $\beta_{\bar{\eta}}$ in (90) is rooted in the overall RG invariance of the potential; i.e.,

$$0 = \left(\frac{\partial}{\partial \log\mu} + \gamma_{\mathscr{M}}\frac{\partial}{\partial\log\mathscr{M}} + \beta_{\bar{\eta}}\frac{\partial}{\partial\bar{\eta}}\right)V_{\mathscr{M}}. \tag{94}$$

Thus, its logarithms may be resummed via

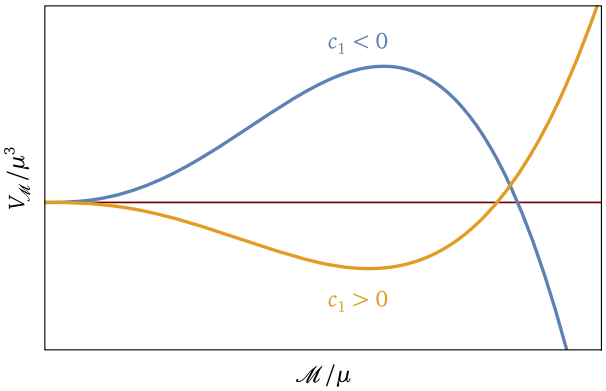

FIG. 5. Schematic dependence of the effective potential at next-to leading order in large-N (91) on the sign of c_1. For $c_1 > 0$, there is a global minimum at $\mathscr{M} \neq 0$, and $V_{\mathscr{M}}$ is bounded from below. With $c_1 < 0$, there is a local minimum $\mathscr{M} = 0$, the global maximum lies at $\mathscr{M} > 0$, and $V_{\mathscr{M}}$ is not bounded from below for $\mathscr{M}/\mu \to \infty$.

$$V_{\mathscr{M}} = \mathscr{M}^3 \exp\left\{\frac{\log(\frac{\mathscr{M}}{\mu})}{1-\gamma_{\mathscr{M}}}\left[3\gamma_{\mathscr{M}} + \beta_{\bar{\eta}}\frac{\partial}{\partial\bar{\eta}}\right]\right\}c_0(\bar{\eta}), \tag{95}$$

where $\gamma_{\mathscr{M}} = \mathcal{O}(N^{-2})$ [7] is the anomalous dimension of the mass operator $\mathscr{M}$ and only contributes at N^{2}LO in the large-N expansion. As a consequence, the logarithmic term arises solely from the LO expression $c_0 = N(1-\bar{\eta})/(24\pi)$.

To argue that the theory remains well defined for $\bar{\eta} \le 1$, we scrutinize the radius of convergence of the effective potential $V_{\mathscr{M}}$. A complication arises due to the series of ring diagrams (61), which are summed into logarithmic series contained in the function $f(\bar{\eta})$ as defined in (63). The radius of convergence for the sum of diagrams is $\bar{\eta} \le 1$, which, strictly speaking, does not permit the exchange the summation and integration as was done to obtain (63). Doing so regardless, we find that $f(\bar{\eta})$ does not exhibit a pole but remains finite as $\bar{\eta} \to 1$. Instead, $f(\bar{\eta})$ develops an imaginary part for $\bar{\eta} > 1$ and so does $V_{\mathscr{M}}$. Imaginary parts of effective potentials are known to be related to their nonconvexity and hint at the coexistance of several ground states. To be precise, the imaginary part is interpreted as a decay rate between well-defined, localized ground states [40,47]. The emergence of an imaginary part in our case can be understood from the fact that we have identified two vacua corresponding to the dynamical masses $M_\pm$ (27), in agreement with [45]. For $\bar{\eta} \le 1$, only M_+ is valid, and there is no imaginary part. M_- becomes a viable vacuum for $\bar{\eta} > 1$, though it is a maximum of the V_{2PI} potential. Thus, $M_\pm$ coexist, but M_+ corresponds to field configurations with lower energy. Thus, there is no imaginary part for V_{eff} computed with $\varphi \neq 0$ in (75), as expected by [17]. On the other hand, $V_{\mathscr{M}}$ is determined at $\varphi = 0$ where $M_\pm$ become degenerate, thus introducing an imaginary part when both vacua coexist at $\bar{\eta} > 1$. Note that this imaginary part of $V_{\mathscr{M}}$ vanishes at the ground state, $\mathscr{M} = 0$, which does not suggest an instability. Furthermore,

the real part of (90) is a smooth function for the coupling values $0 \leq \bar{\eta} \leq \bar{\eta}^*$. Thus, the imaginary part does not pose a problem to our conclusion.

The consequence of our finding is profound: Scale invariance cannot be broken by the BMB phenomenon, as it is inherently broken by quantum fluctuations, concretely by the logarithmic term in (91). Quantum corrections fix the ground state to $\mathscr{M} = 0$, and the effective potential of the mass parameter $\mathscr{M}$ cannot be rendered flat for any value of $\bar{\eta}$. Thus, no dimensional transmutation occurs, and the BMB mechanism utterly disappears in the face of NLO corrections.

A similar conclusion can be drawn by considering the gap equation. At NLO, it reads diagrammatically

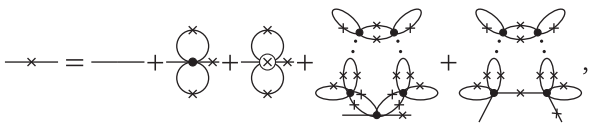

(96)

where the small dots denote arbitrarily many insertions of the same shape, and $\otimes$ denotes the sextic tree-level counterterm insertion. The last family of diagrams in (96) yields an explicit dependence on the external momentum. Hence, the gap equation at NLO does not merely describe a dynamical mass parameter but rather a more complicated dressed propagator.

Setting aside this complication, the dynamical mass parameter $\mathscr{M}$ gains additional contributions with respect to the LO condition (77)

$$\mathscr{M}^2 = \mathscr{M}^2 \left[\bar{\eta} + \beta_{\bar{\eta}} \log \frac{\mathscr{M}}{\mu} + \ldots \right], \tag{97}$$

which only permits the solution $\mathscr{M} \propto \mu$ as well as the ground state $\mathscr{M} = 0$.

As $V_{\mathscr{M}}$ is not a flat function of $\mathscr{M}$, the composite field (82) ceases to be a dilaton. We will not compute explicit corrections to its LO mass (84) as it will vanish due to $\mathscr{M} = 0$. Note that the authors of [28] have employed saddle point methods to argue that for $\mathscr{M} \neq 0$, the mass is tachyonic at $\bar{\eta} = 1$. A cross-check of this result is beyond the scope of this work.

V. CONCLUSIONS

In this work, we revisited the $O(N)$ model with ϕ^6 interactions using perturbation theory, dimensional regularization, and minimal subtraction. Through resummations, we derived exact expressions in a systematic $1/N$ expansion, which we used as a guardrail into strongly coupled regimes. We also employed composite-operator effective-action techniques to track possible competing vacua. This set of tools allowed us to reconcile and extend various literature results, including those obtained via saddle point approximations or the FRG.

Each of our findings supports the conclusion that the UV fixed point found in [5–7] exists and is accessible within a weakly coupled regime for realistic QFTs at large N. Concretely, we demonstrated that the fixed point becomes vanishingly small in a $N \to \infty$ limit, which ensures its persistence to higher-loop orders in the β function. This is an extension to the arguments brought forth in [6,7], which leaves no room for doubt about the viability of the perturbative expansion. Moreover, we computed the first complete expression for the effective potential at NLO in the $1/N$ expansion, superseding any partial attempts in prior literature [16,44]. Our results suggest that for sufficiently large N, the fixed point is stable as spontaneous breaking of the global $O(N)$ symmetry does not occur. Furthermore, we showed that the tricritical line of conformality does not interfere with the existence of the UV fixed point; its well-known disappearance [19,20,25,30,32] is the consequence of a consistent $1/N$ expansion. Finally, we brought forward new arguments that show the absence of the BMB instability [22] at NLO. Thus, there is no evidence for any obstructions to the UV fixed point.

Our findings suggest that both the tricritical line of conformality, as well as the BMB phenomenon at its end point, are ephemeral products of a strict $N \to \infty$ limit. They are based on an accidental scale invariance only present at LO in the $1/N$ expansion, which is broken by quantum fluctuations in realistic large-N QFTs. We interpret this LO scale invariance as a relict of the classical scale symmetry. Once quantum corrections are fully accounted for, the scale invariance is broken and only restored at the UV fixed point [5–7].

We expect that the results of this paper, including the persistence of Pisarski's fixed point, can be corroborated using the FRG, provided a sufficiently nuanced truncation is employed. We leave this exploration to future work.

ACKNOWLEDGMENTS

We are indebted to E. Stamou for comments on the manuscript. We thank C. Cresswell–Hogg, D. F. Litim, M. M. Scherer, and Y. Schröder for discussions. M. U. is supported by the doctoral scholarship program of the *Studienstiftung des deutschen Volkes* and the Mercator Research Center Ruhr under Project No. Ko-2022-0012. The work of S. K. has been funded by Consejería de Universidad, Investigación e Innovación, Gobierno de España and Unión Europea—NextGenerationEU under Grants No. AST22 6.5 and CNS2022-136024 and by MICIU/AEI/10.13039/501100011033 and FEDER/UE (Grant No. PID2022-139466NB-C21).

DATA AVAILABILITY

No data were created or analyzed in this study.

APPENDIX: DETAILS ON MULTILOOP INTEGRALS IN LARGE N

In this appendix, we collect the relevant techniques and provide further details on the multiloop integrals that appear in the main text. We always work in the minimal subtraction scheme and regularize loop integrals in $d = 3 - 2\varepsilon$ dimensions. To evaluate the integrals, we employ the `MaRTIn` [48] framework, which in turn uses `QGRAF` [49] for diagram generation and `FORM` [50] for the symbolic computations.

As we compute the effective potential at leading order (LO) and next-to-leading order (NLO) in a $1/N$ expansion, an infinite amount of loop diagrams has to be resummed. The LO contributions take the form of tadpoles (15), which factorize and are finite. They can be resummed by introducing a dynamical mass parameter that can be determined via a gap equation (25). Explicitly, the tadpoles $\mathcal{T}$ are finite and read

$$\mathcal{T} = \bigcirc\!\!\bullet = \int \frac{\mathrm{d}^d k}{(2\pi)^d} \frac{1}{k^2 - m^2} = -\frac{i|m|}{(4\pi)^{3/2}} \left(\frac{\mu^2}{|m|^2} e^{\gamma_E} \right)^{\varepsilon} \Gamma\left(\varepsilon - \frac{1}{2}\right) = \frac{i|m|}{4\pi} + \mathcal{O}(\varepsilon). \tag{A1}$$

At NLO, there are sets of ring diagrams R_n (57) and $\tilde{R}_n$ (65), which cannot be resummed by the same means. They incorporate chains of subgraphs (56), which contain one-loop bubble diagrams that explicitly depend on the momentum routed through them from external legs. In general d dimensions, each of these bubbles $\mathcal{B}$ reads

$$\mathcal{B} = \bullet\!\!\bigcirc\!\!\bullet = \int \frac{\mathrm{d}^d k}{(2\pi)^d} \frac{1}{(k^2 - m^2)((k+p)^2 - m^2)}. \tag{A2}$$

Using Feynman parametrisation, Wick rotation, and standard integration methods, we arrive at

$$\mathcal{B} = \frac{i}{4\pi p_E} \arctan\left(\frac{p_E}{2m}\right) + \mathcal{O}(\varepsilon), \tag{A3}$$

where p_E is the Euclidean momentum. We find this expression to be in agreement with [51].

The diagrams $\tilde{R}_{1,1}$ (67), R_2 (59), and R_3 (60) are UV divergent and can be directly obtained by combining the respective two-loop [52], three-loop [53], and four-loop integrals [54] and factorizing LO tadpoles (A1). The remaining diagrams $R_{n\geq 4}$ (61), $\tilde{R}_{1,l\geq 2}$ (68), and $\tilde{R}_{n\geq 2}$ (69) are finite. We have opted to sum them as the common expression $\sum_{n=4}^{\infty} R_n + \sum_{n=2}^{\infty} (\tilde{R}_{1,l} + \tilde{R}_n)$ in (70), introducing the function $F(x)$ as defined in (71), which encapsulates the integration over the bubble momentum p_E from (A3). In the effective potential at NLO (75), the evaluation of $F(x)$ is performed numerically.

To obtain the result for $V_{\mathscr{M}}$ (90), merely a resummation of $R_{n\geq 4}$ is required, which is abbreviated as (62) introducing the function $f(x)$ in the same manner as before (63). This function $f(x)$ has a finite the radius of convergence for positive arguments $x \leq 1$, which stems from the sum $\sum_n R_n$ being divergent. Thus, $f(x)$ is only well defined within this radius of convergence, as it relies on exchanging the summation of diagrams and individual loop integrations. As before, $f(x)$ is evaluated numerically to discuss (90).

While we have found the numerical evaluation of the summed expression $\sum_{n=4}^{\infty} R_n$ (62) to be more practical, we could have chosen to compute each of the contributions R_n (61) analytically. For $n \geq 4$, they can be written as

$$R_n = -\frac{2M^3}{\pi^2 n} \left[\bar{\eta} \left(1 - \frac{4\pi\varphi^2}{NM} \right) \right]^n I_n, \tag{A4}$$

where the integral I_n defined as

$$I_n = \int_0^{\infty} \frac{\arctan^n(z)}{z^{n-2}} \mathrm{d}z \tag{A5}$$

can be obtained recursively. After repeated integration by parts, we can write down I_n in terms of base integrals J_n, which are defined below and can be integrated more easily. As expressions differ slightly depending on whether n is odd or even, we use superscripts I_n^{odd} and I_n^{even} to discriminate between the two cases. The integral I_n can reduced in a recursion

$$I_n^{\mathrm{odd}} = \frac{n}{n-3} [I_{n-1}^{\mathrm{even}} + (-1)^{(n-1)/2} J_{n-1}^{\mathrm{even}} + \mathcal{S}_{n-1}^{\mathrm{even}}(n-5)], \quad n > 5, \tag{A6}$$

$$I_n^{\mathrm{even}} = \frac{n}{n-3} [I_{n-1}^{\mathrm{odd}} + (-1)^{n/2} J_{n-1}^{\mathrm{odd}} + \mathcal{S}_{n-1}^{\mathrm{odd}}(n-5)], \quad n > 4, \tag{A7}$$

which is terminated at the lowest cases of n, where the integrals read

$$I_4 = 4J_3, \quad \text{and} \quad I_5 = \frac{5}{2} J_4. \tag{A8}$$

Here, $\mathcal{S}_n$ are recursive sums defined via

$$\mathcal{S}_n^{\text{odd}}(m) = \sum_{k=1}^{(m-1)/2} \frac{(-1)^{(m-2k-1)/2} n}{2k} \left((-1)^k J_{n-1}^{\text{even}} + \mathcal{S}_{n-1}^{\text{even}}(2k)\right), \quad m \geq 3, \tag{A9}$$

$$\mathcal{S}_n^{\text{even}}(m) = \sum_{k=2}^{m/2} \frac{(-1)^{(m-2k)/2} n}{2k-1} \left((-1)^k J_{n-1}^{\text{odd}} + \mathcal{S}_{n-1}^{\text{odd}}(2k-1)\right), \quad m \geq 4. \tag{A10}$$

After performing all recursions, only base integrals J_n remain, which can be computed directly and are defined as

$$J_n^{\text{odd}} = \int_0^\infty \frac{\arctan^n(z)}{z(1+z^2)} \mathrm{d}z = \left(\frac{\pi}{2}\right)^n \log 2 + \sum_{m=1}^{(n-1)/2} (-1)^m \left(\frac{\pi}{2}\right)^{n-2m} \frac{(2^{2m}-1)}{2^{4m}} \frac{n! \zeta_{2m+1}}{(n-2m)!}, \tag{A11}$$

for odd values of n, whereas J_n for even n is related to the J_n^{odd} by

$$J_n^{\text{even}} = \int_0^\infty \frac{\arctan^n(z)}{z^2(1+z^2)} \mathrm{d}z = -\frac{1}{(n+1)} \left(\frac{\pi}{2}\right)^{n+1} + n J_{n-1}^{\text{odd}}. \tag{A12}$$

[1] M. Blume, V. J. Emery, and R. B. Griffiths, Ising model for the λ transition and phase separation in $He^3 - He^4$ mixtures, Phys. Rev. A **4**, 1071 (1971).

[2] C. A. Aragao de Carvalho, A Callan-Symanzik study of the $\lambda\phi^4$ in three-dimensions + $g\phi^6$ in three-dimensions theory, Nucl. Phys. **B119**, 401 (1977).

[3] R. Alben, Nematic-smectic transitions in mixtures—a liquid crystal tricritical point, Solid State Commun. **13**, 1783 (1973).

[4] B. M. Ocko, R. J. Birgeneau, J. D. Litster, and M. E. Neubert, Critical and tricritical behavior at the nematic to smectic-*A* transition, Phys. Rev. Lett. **52**, 208 (1984).

[5] P. K. Townsend, Consistency of the $1/n$ expansion for three-dimensional ϕ^6 theory, Nucl. Phys. **B118**, 199 (1977).

[6] T. Appelquist and U. W. Heinz, Three-dimensional O(N) theories at large distances, Phys. Rev. D **24**, 2169 (1981).

[7] R. D. Pisarski, Fixed point structure of ϕ^6 in three-dimensions ar large N, Phys. Rev. Lett. **48**, 574 (1982).

[8] K. Gawedzki and A. Kupiainen, Renormalizing the non-renormalizable, Phys. Rev. Lett. **55**, 363 (1985).

[9] B. Rosenstein, B. J. Warr, and S. H. Park, The four fermi theory is renormalizable in $(2+1)$-dimensions, Phys. Rev. Lett. **62**, 1433 (1989).

[10] G. Gat, A. Kovner, B. Rosenstein, and B. J. Warr, Four Fermi interaction in $(2+1)$-dimensions beyond leading order in $1/N$, Phys. Lett. B **240**, 158 (1990).

[11] D. F. Litim and F. Sannino, Asymptotic safety guaranteed, J. High Energy Phys. 12 (**2014**) 178.

[12] D. F. Litim, M. Mojaza, and F. Sannino, Vacuum stability of asymptotically safe gauge-Yukawa theories, J. High Energy Phys. 01 (2016) 081.

[13] A. D. Bond, D. F. Litim, and T. Steudtner, Asymptotic safety with Majorana fermions and new large N equivalences, Phys. Rev. D **101**, 045006 (2020).

[14] D. F. Litim, N. Riyaz, E. Stamou, and T. Steudtner, Asymptotic safety guaranteed at four-loop order, Phys. Rev. D **108**, 076006 (2023).

[15] T. Steudtner, Effective potential and vacuum stability in the Litim-Sannino model, J. High Energy Phys. 05 (2024) 149.

[16] P. K. Townsend, Spontaneous symmetry breaking in $O(n)$ symmetric ϕ^6 theory in the $\frac{1}{N}$ expansion, Phys. Rev. D **12**, 2269 (1975).

[17] P. K. Townsend, The global ground state of ϕ^6 theory in three-dimensions, Phys. Rev. D **14**, 1715 (1976).

[18] T. Appelquist and U. W. Heinz, Vacuum stability in three-dimensional O(N) theories, Phys. Rev. D **25**, 2620 (1982).

[19] F. David, D. A. Kessler, and H. Neuberger, The Bardeen-Moshe-Bander fixed point and the ultraviolet triviality of ϕ^6 in three-dimensions, Phys. Rev. Lett. **53**, 2071 (1984).

[20] F. David, D. A. Kessler, and H. Neuberger, A study of $(\phi^2)^3$ in three-dimensions at $N = \infty$, Nucl. Phys. **B257**, 695 (1985).

[21] D. F. Litim, E. Marchais, and P. Mati, Fixed points and the spontaneous breaking of scale invariance, Phys. Rev. D **95**, 125006 (2017).

[22] W. A. Bardeen, M. Moshe, and M. Bander, Spontaneous breaking of scale invariance and the ultraviolet fixed point in O(N) symmetric $(\phi^6)_3$ theory, Phys. Rev. Lett. **52**, 1188 (1984).

[23] J. S. Hager, Six-loop renormalization group functions of O(n)-symmetric ϕ^6-theory and epsilon-expansions of tricritical exponents up to ϵ^3, J. Phys. A **35**, 2703 (2002).

[24] R. Shrock, Study of the ultraviolet behavior of an O(N)ϕ^6 theory in $d = 3$ dimensions, Phys. Rev. D **107**, 096009 (2023).

[25] D. J. Amit and E. Rabinovici, Breaking of scale invariance in ϕ^6 theory: Tricriticality and critical end points, Nucl. Phys. **B257**, 371 (1985).

[26] R. Gudmundsdottir, G. Rydnell, and P. Salomonson, On $1/N$ expansion in $(\phi^2)^2$ in three-dimensions field theory, Ann. Phys. (N.Y.) **162**, 72 (1985).
[27] R. Gudmundsdottir, G. Rydnell, and P. Salomonson, More on $O(N)$ symmetric ϕ^6 in three-dimensions theory, Phys. Rev. Lett. **53**, 2529 (1984).
[28] H. Omid, G. W. Semenoff, and L. C. R. Wijewardhana, Light dilaton in the large N tricritical $O(N)$ model, Phys. Rev. D **94**, 125017 (2016).
[29] T. R. Morris and M. D. Turner, Derivative expansion of the renormalization group in O(N) scalar field theory, Nucl. Phys. **B509**, 637 (1998).
[30] S. Yabunaka and B. Delamotte, Surprises in $O(N)$ models: Nonperturbative fixed points, large N limits, and multicriticality, Phys. Rev. Lett. **119**, 191602 (2017).
[31] D. F. Litim and M. J. Trott, Asymptotic safety of scalar field theories, Phys. Rev. D **98**, 125006 (2018).
[32] C. Fleming, B. Delamotte, and S. Yabunaka, Finite N origin of the Bardeen-Moshe-Bander phenomenon and its extension at $N = \infty$ by singular fixed points, Phys. Rev. D **102**, 065008 (2020).
[33] C. Bollini and J. Giambiagi, Lowest order "divergent graphs" in ν-dimensional space, Phys. Lett. **40B**, 566 (1972).
[34] C. Bollini and J. Giambiagi, Dimensional renormalization: The number of dimensions as a regularizing parameter, Nuovo Cimento Soc. Ital. Fis. **12B**, 20 (1972).
[35] G. 't Hooft, Dimensional regularization and the renormalization group, Nucl. Phys. **B61**, 455 (1973).
[36] W. A. Bardeen, A. Buras, D. Duke, and T. Muta, Deep inelastic scattering beyond the leading order in asymptotically free gauge theories, Phys. Rev. D **18**, 3998 (1978).
[37] D. G. C. McKeon and G. Tsoupros, Perturbative evaluation of renormalization group functions in massive three-dimensional ϕ^6 theory, Phys. Rev. D **46**, 1794 (1992).
[38] S. R. Coleman and E. J. Weinberg, Radiative corrections as the origin of spontaneous symmetry breaking, Phys. Rev. D **7**, 1888 (1973).
[39] R. Jackiw, Functional evaluation of the effective potential, Phys. Rev. D **9**, 1686 (1974).
[40] M. Sher, Electroweak Higgs potentials and vacuum stability, Phys. Rep. **179**, 273 (1989).
[41] W. A. Bardeen and M. Moshe, Phase structure of the O(N) vector model, Phys. Rev. D **28**, 1372 (1983).
[42] D. F. Litim and E. Marchais, Critical $O(N)$ models in the complex field plane, Phys. Rev. D **95**, 025026 (2017).
[43] H. Osborn and A. Stergiou, Seeking fixed points in multiple coupling scalar theories in the ϵ expansion, J. High Energy Phys. 05 (2018) 051.
[44] Y. Matsubara, T. Suzuki, and I. Yotsuyanagi, Is large-N $(\phi^6)_3$ theory still mathematically inconsistent?, Z. Phys. C **27**, 599 (1985).
[45] Y. Matsubara, T. Suzuki, H. Yamamoto, and I. Yotsuyanagi, On a phase with spontaneously broken scale invariance in three dimensional O(N) models, Prog. Theor. Phys. **78**, 760 (1987).
[46] J. M. Cornwall, R. Jackiw, and E. Tomboulis, Effective action for composite operators, Phys. Rev. D **10**, 2428 (1974).
[47] E. J. Weinberg and A.-q. Wu, Understanding complex perturbative effective potentials, Phys. Rev. D **36**, 2474 (1987).
[48] J. Brod, L. Hüdepohl, E. Stamou, and T. Steudtner, MaRTIn—manual for the "massive recursive tensor integration", Comput. Phys. Commun. **306**, 109372 (2025).
[49] P. Nogueira, Automatic Feynman graph generation, J. Comput. Phys. **105**, 279 (1993).
[50] J. Kuipers, T. Ueda, J. A. M. Vermaseren, and J. Vollinga, FORM version 4.0, Comput. Phys. Commun. **184**, 1453 (2013).
[51] A. V. Kotikov, Some examples of calculation of massless and massive feynman integrals, Particles **4**, 361 (2021).
[52] A. I. Davydychev and J. B. Tausk, Two loop selfenergy diagrams with different masses and the momentum expansion, Nucl. Phys. **B397**, 123 (1993).
[53] A. K. Rajantie, Feynman diagrams to three loops in three-dimensional field theory, Nucl. Phys. **B480**, 729 (1996).
[54] R. N. Lee and I. S. Terekhov, Application of the DRA method to the calculation of the four-loop QED-type tadpoles, J. High Energy Phys. 01 (2011) 068.